Available online at www.sciencedirect.com

ScienceDirect

ARTICLE

Fabrication of g-C₃N₄/MoS₂ Nanosheet Heterojunction by Facile Ball Milling Method and Its Visible Light Photocatalytic Performance

Yan Xin[1],   Gao Qiang[1],   Hui Xiaoyan[1],   Yan Congxiang[1],   Ai Tao[1],   Wang Zhenjun[1,2],

Sun Guodong[1],   Su Xinghua[1],   Zhao Peng[1]

[1] Chang'an University, Xi'an 710064, China; [2] Engineering Research Center of Pavement Materials, Ministry of Education, Xi'an 710064, China

Abstract: The g-C₃N₄/MoS₂ nanosheet heterojunction was prepared via a facile ball milling method. The microstructure and morphology of the composite were characterized by X-ray diffraction (XRD), high-resolution transmission electron microscopy (HRTEM), UV-vis diffuse reflectance spectroscopy (DRS) and photoluminescence (PL) spectroscopy. The photocatalytic activities were evaluated by the degradation of organic Rhodamine B (RhB) under visible light irradiation. The results indicate that MoS₂ nanosheets are successfully coupled into g-C₃N₄ to form a C₃N₄/ MoS₂ heterojunction. The kinetic constant of RhB degradation with g-C₃N₄/MoS₂ nanosheets-2 wt% heterojunction (0.0368 min^{-1}) is about 4.3 times as high as that of the bulk g-C₃N₄ (0.00840 min^{-1}). The enhanced photocatalytic activities can be mainly ascribed to the efficient separation and transportation of photo-induced electron-hole pairs. The possible photocatalytic mechanism of composites was proposed according to the light trapping experiment.

Key words: MoS₂ nanosheets; graphite phase carbon nitride; heterojunction; ball milling; visible light photocatalysis

Semiconductor photocatalysis has been developed as a kind of green technology for controlling environmental pollutants because of their semiconducting characteristics and commercial availability[1,2]. Many semiconductor materials, such as TiO₂, WO₃, CdS, ZnS and ZnO, have been investigated as photocatalysts for the degradation of organic compounds[3-7]. However, various shortcomings, such as low utilization of visible light and high recombination rate of the photo-generated electron-hole pairs greatly restrict the efficiency of these photocatalysts. Therefore, it has become a hot issue in photocatalysis field to explore more efficient visible light catalysts for meeting the requirement of practical applications.

Recently, the graphite phase carbon nitride (g-C₃N₄) have attracted much attention in hydrogen production by water splitting and degradation of pollutants under visible light irradiation[8-11]. The g-C₃N₄ has many advantages such as good chemical stability, a band gap of 2.7 eV as well as layered structure. Nevertheless, the photocatalytic performance of bulk g-C₃N₄ is limited due to the fast recombination of photo-generated electron-hole pairs and a small specific surface area. More studies have showed that the g-C₃N₄-based heterojunction structure can obviously increase the photocatalytic efficiency by improving the electron-hole pair separation efficiency[12-16]. MoS₂ nanosheets have many unique optical and electrical properties compared with its bulk structure. MoS₂ nanosheets can construct the semiconductor heterojunction with g-C₃N₄ due to a suitable band gap of 1.9 eV, large specific surface area and more unsaturated bonds on the surface of MoS₂ nanosheets[17-25]. Lu et al[26] used a bathing and ultrasound method to prepare graphitic C₃N₄/ultrathin MoS₂ hybrids for organic degradation, which accelerate the

separation of photo-generated electron-hole pairs. Hou et al[27] constructed a porous g-C$_3$N$_4$ nanosheets, N-doped graphene, and layered MoS$_2$ ternary heterojunction by a hydrothermal method. The ternary heterojunction shows significantly enhanced photocatalytic activities owing to the large specific surface area, enhanced visible light absorption, and fast electron-hole pair separation and transfer. However, in these works, g-C$_3$N$_4$/MoS$_2$ photocatalyst heterojunction was synthesized at high temperature or by a complicate synthesis process. It is still necessary to explore a facile, low energy consumption and effective methods to obtain g-C$_3$N$_4$/MoS$_2$ heterojunction composites with high photocatalytic efficiency.

In this study, the g-C$_3$N$_4$/MoS$_2$ nanosheet heterojunction photocatalysts were prepared by a ball milling method. Compared with other composite preparation methods, ball milling is a simple and mass preparation technique to synthesize composite photocatalysts. The resultant composite photocatalysts exhibited enhanced visible light photocatalytic activities by RhB degradation. A possible photocatalytic mechanism of the composite photocatalysts was also proposed.

1　Experiment

The bulk g-C$_3$N$_4$ (BCN) powder was synthesized by directly heating melamine according to a reported method[8]. 10 g melamine powder was heated to 520 ^{o}C in a muffle furnace with a rate of 5 ^{o}C/min for 4 h. After the reaction, the resultant g-C$_3$N$_4$ was collected and ground into powders for further use.

MoS$_2$ nanosheets (MSNs) were prepared by a two-step procedure in modified methods 6 the Ref. [28]. Firstly, 2 g of MoS$_2$ powder was dispersed in 200 mL N-methyl-2-pyrrolidone (NMP) and the mixture was put in a sealed polypropylene bottle with 500 zirconia balls. The milling speed was set to 100 r/min. The milling time was 24 h. Secondly, the samples were further subjected to ultrasonic treatment at low power output (100 W) for 2 h. Then layered MoS$_2$ nanosheets were prepared in NMP solutions.

The preparation of g-C$_3$N$_4$/MoS$_2$ nanosheet heterojunction photocatalyst was achieved in QM-3SP04 ball mill. The details of the procedure were as follows: the g-C$_3$N$_4$ powders were put together with a certain amount of MoS$_2$ nanosheet solutions, and then the agate balls were mixed in the agate jar at a mass ratio of 1:10. After milling at a speed of 400 r/min for 4 h, the final products were washed and dried in a vacuum oven at 80 ^{o}C for 10 h. The obtained g-C$_3$N$_4$/MoS$_2$ nanosheet heterojunction photocatalyst with different MoS$_2$ mass fractions of 0.5%, 1%, 2% and 3% were donated as BCNMSNs-0.5, BCNMSNs-1, BCNMSNs-2 and BCNMSNs-3, respectively. The sample named M-BCNMSNs-2 (2 wt% MoS$_2$) was obtained by directly mixing the MoS$_2$ nanosheets with g-C$_3$N$_4$.

The crystalline phases of the samples were analyzed by X-ray diffraction (XRD, Bruker D8 Advance X-ray diffractometer)

with Cu Kα radiation source. The morphologies of the samples were characterized by transmission electron microscopy (TEM, Tecnai G20). The UV-vis diffuse reflectance spectra (UV-vis DRS) were obtained by UV-vis spectrophotometer (Shimadzu, UV-3600) with BaSO$_4$ as a reflectance standard. The photoluminescence spectra were obtained on a HORIBA Fluorolog-3 type fluorescence spectrophotometer with an excitation wavelength of 270 nm.

The photocatalytic performance of the samples was evaluated by the degradation of the organic RhB by a 300 W Xe lamp with a cutoff filter (λ>420 nm). In a typical photocatalytic experiment, 20 mg of photocatalyst was added into 100 mL of the RhB solution (20 mg/L), and then the solution was stirred in the dark for 30 min to establish an adsorption-desorption equilibrium before visible light irradiation. Next, 3 mL of the solution was collected at a given time interval, and then centrifuged (10 000 r/min, 5 min) to remove the particles. The concentration of RhB was determined at the 553 nm absorbance value.

The trapping experiments were performed according to the Ref. [29-31]. 0.1 mL of isopropanol (IPA), 0.1 g of benzoquinone (BQ) and 0.1 g of ammonium oxalate (AO) were added to the RhB solution for photocatalytic degradation.

2　Results and Discussion

2.1　Crystallization phase structure and morphology of the composite photocatalysts

Fig.1 depicts the XRD patterns of bulk g-C$_3$N$_4$, MoS$_2$ nanosheets and g-C$_3$N$_4$/ MoS$_2$ nanosheet heterojunctions with different MoS$_2$ contents. There are two distinct peaks (27.5^o and 13.1^o) in bulk g-C$_3$N$_4$. It can be indexed as the (002) and (100) diffraction planes of the g-C$_3$N$_4$ (JCPDS 87-1526). The strong peak at 27.5^o is related to the inter-layer stacking of aromatic systems and the weak peak at 13.1^o corresponds to the in-plane structural packing motif. Moreover, the peak of MoS$_2$ nanosheets at 14.3°, 32.6°, 33.4°, 35.8°, 39.4°, 44.1°, 58.2° and 60.2° are assigned to the hexagonal structure of MoS$_2$ (JCPDS No.37-1492). The diffraction peaks indicate that the MoS$_2$ nanosheets still keep well crystallinity after ball
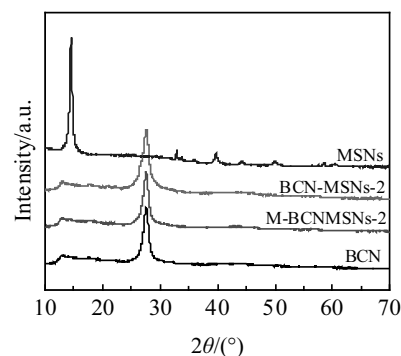

Fig.1　XRD patterns of BCN, MSNs, M-BCNMSNs-2 and BCN-MSNs-2

milling and ultrasonic exfoliation. The diffraction peak positions of the M-BCNMSNs and BCN-MSNs samples are similar to those of g-C_3N_4. The results indicate that MoS_2 nanosheets do not incorporate into the g-C_3N_4 lattice. There are no apparent peaks of MoS_2 in the M-BCNMSNs and BCN-MSNs, because the MoS_2 content is lower.

Fig.2a shows a high-resolution TEM image of MoS_2 nanosheets. The MoS_2 nanosheets consist of several atomic layers (3 layer). The lattice spacing (d=0.62 nm) corresponds to the (002) plane of MoS_2. Fig.2b shows the TEM image of the g-C_3N_4/MoS_2 nanosheets-2% composite. The MoS_2 nanosheets are inserted onto the layered structure of the g-C_3N_4. The selected region marked by the white circle in Fig.2b is magnified to investigate the fine structure of the g-g-C_3N_4/MoS_2 nanosheets-2% composite (Fig.2c). The magnified TEM image shows the formation of MoS_2 nanosheets/g-C_3N_4 heterojunction with intimate interfacial contact. In particular, the bulk g-C_3N_4 can be exfoliated during the ball milling and ultrasonic procedure.

2.2 DRS and PL analyses

The UV-vis diffuse reflectance spectra of bulk g-C_3N_4 and g-C_3N_4/MoS_2 nanosheets with different MoS_2 contents are shown in Fig.3. The bulk g-C_3N_4 sample displays absorption from the ultraviolet to the visible range up to 460 nm, which can be ascribed to the small band gap of bulk g-C_3N_4. The

M-BCNMSNs-2 sample shows the same absorption edge as bulk g-C_3N_4, indicating that MoS_2 nanosheets do not influence g-C_3N_4 structure through the simple physical mixing method. However, compared with bulk g-C_3N_4, the absorption edge of the BCN-MSNs sample presents a red shift. At the same time, the absorption peak intensity above 450 nm is enhanced with increasing MoS_2 contents. The results imply that MoS_2 nanosheets are successfully coupled into g-C_3N_4 to form a g-C_3N_4/MoS_2 heterojunction by ball mill process. Therefore, the g-C_3N_4/MoS_2 heterojunction can capture more visible light and enhance catalytic activity.

The separation and recombination of photogenerated electron-hole pairs is very important to the performance of the catalyst. The photoluminescence spectra can be used to reveal the separation and recombination of photogenerated charges in semiconductor materials. Fig.4 shows the PL spectra of bulk g-C_3N_4 and g-C_3N_4/MoS_2 nanosheets with different MoS_2 contents. The bulk g-C_3N_4 has a strong fluorescence emission peak near 465 nm, which is consistent with the absorption boundary of g-C_3N_4 in the UV-Vis spectrum[32]. The results show that the photogenerated electron-hole pairs are easy to combine in bulk g-C_3N_4, which is not conducive to its photo-catalytic performance. The mechanical mixture of g-C_3N_4/MoS_2 nanosheets shows high PL emission intensity, which means that the sample still maintains a higher recombination
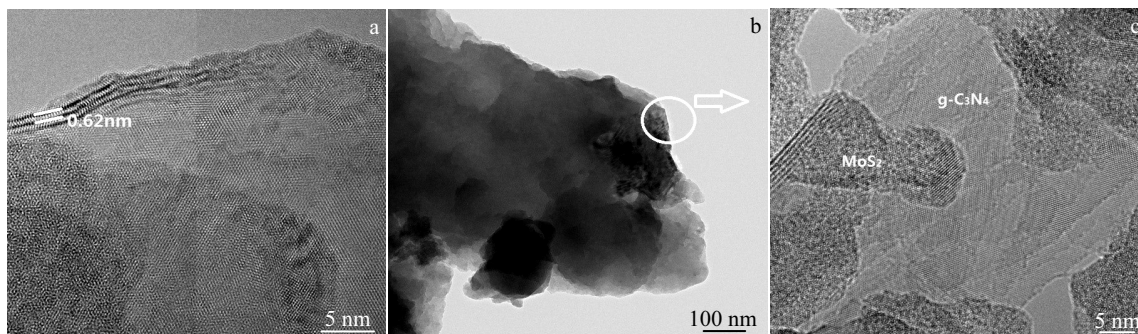

Fig.2 HR-TEM images of MSNs (a), TEM image of BCN-MSNs-2 (b), and HR-TEM image of marked region in Fig.2b (c)
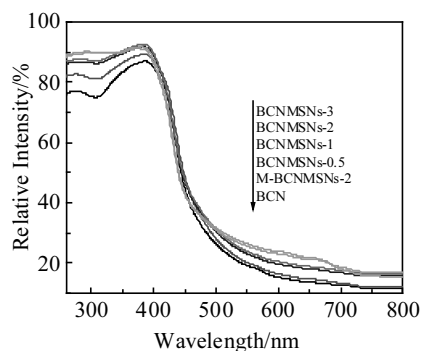

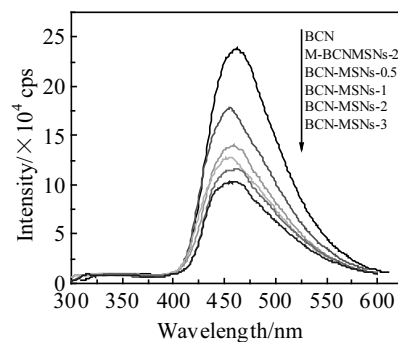Fig.3 UV-vis diffuse reflectance spectra of different samples

Fig.4 PL spectra of different samples with an excitation wavelength of 270 nm

rate of photo-generated charges. The intensities of PL spectra for g-C_3N_4/MoS_2 nanosheets composites decrease with increasing MoS_2 content, which indicates that the separation efficiency of photo-induced charges in the composites is obviously improved.

2.3 Photocatalytic activities analyses

The photocatalytic activities of the different samples were evaluated by the degradation of RhB under visible light irradiation, as shown in Fig.5. The RhB is degraded by nearly 3.2% at 120 min without catalyst, suggesting that the effect of self-photo degradation for RhB is limited. The bulk g-C_3N_4 sample shows visible light photocatalytic activity. After 120 min of visible light illumination, the RhB has been degraded by about 63%. The mechanical mixture g-C_3N_4/MoS_2 nanosheets only degrades 70% of RhB after 120 min of visible light illumination. The results show that only simple mechanical mixing of MoS_2 nanosheets with g-C_3N_4 cannot improve photocatalytic performance of bulk g-C_3N_4. Compared with the bulk g-C_3N_4 and the mechanical mixture of g-C_3N_4/MoS_2 nanosheets, the g-C_3N_4/MoS_2 nanosheet composite catalyst exhibits excellent photocatalytic activity. The BCNMNs-2 composites result in a 98% degradation of RhB within 120 min. For low concentration pollutants, the kinetics behaviors for the degradation reaction can be studied by the equation:

$$\ln\left(C/C_0\right) = kt \tag{1}$$

where C is the concentration of the pollutant degradated by photocatalyst (mg·L^{-1}), C_0 is the adsorption equilibrium concentration of the pollutant before irradiation (mg·L^{-1}), t is the reaction time (min), and k is the kinetic constant (min^{-1}). The kinetic constants (k) of different samples are calculated and shown in Fig.6. The kinetic constant of RhB degradation with BCNMSNs-2 (0.0368 min^{-1}) is about 4.3 and 3.8 times as high as that of the BCN (0.008 40 min^{-1}) and M-BCNMSNs-2 (0.009 69 min^{-1}), respectively. The results show that the formation of MoS_2 nanosheets/g-C_3N_4 heterojunction can efficiently enhance the photocatalytic performance of g -C_3N_4.
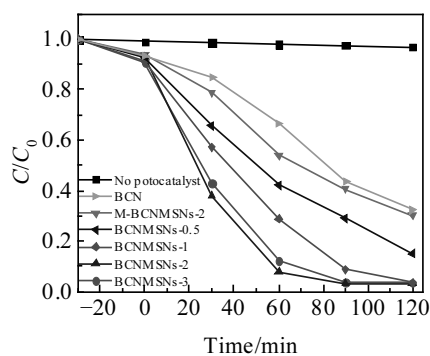
Fig.5   Photocatalytic degradation of RhB as a function of irradiation time for different samples under visible light irradiation
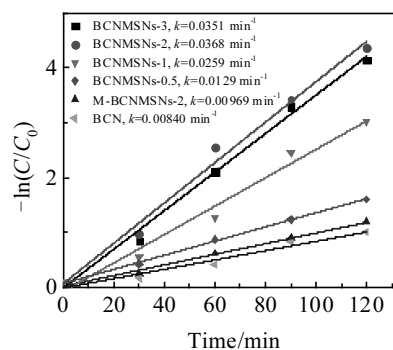
Fig.6   Kinetic plots of photocatalytic degradation of RhB for different samples under visible light irradiation

2.4 Photocatalytic mechanism of MoS_2 nanosheets/g-C_3N_4 heterojunction

To investigate the photocatalytic mechanism of the g-C_3N_4/MoS_2 nanosheet heterojunction with 2 wt% MoS_2, the trapping experiments of the photocatalysts were carried out for determining the main active species. The scavengers used in this study are AO for holes (h^+), IPA for hydroxyl radicals (•OH) and BQ for superoxide radicals (•O_2−). The results are shown in Fig.7. The degradation rate (η) of RhB obviously decreases with the addition of AO compared to the use of IPA and BQ. It manifests that holes play a main role in the RhB degradation process, while hydroxyl radicals and superoxide radicals can be negligible in the reaction. According to the above results, the possible mechanism of the g-C_3N_4/MoS_2 nanosheet heterojunction is illustrated in Fig.8. The electrons from the valence bands (VBs) of g-C_3N_4 and MoS_2 nanosheets are excited to their respective conduction bands (CBs) under the visible light irradiation, which simultaneously create holes in the VB. The CB and VB edge potentials of the bulk g-C_3N_4 are –1.13 eV and +1.57 eV, respectively[33]. The CB and VB edge potentials of MoS_2 nanosheets are –0.12 eV and +1.78 eV[34], respectively. The CB and VB edge potentials of MoS_2 nanosheets are more positive than that of g-C_3N_4. Therefore, the photo-induced electrons from the CB of g-C_3N_4 particle move to the CB of MoS_2 nanosheets through heterojunction interface in this sample. As reported[26,35], the MoS_2 nanosheets show higher electron mobility than bulk MoS_2, which is beneficial to the transferring photogenerated charges. At the same time, the holes in the VB of the MoS_2 nanosheets can be transferred to the g-C_3N_4 by the internal static electric fields. Consequently, the electrons are gathered in the CB of the MoS_2 and the holes in the VB of the g-C_3N_4. However, the electrons in the CB of the MoS_2 (–0.12 eV) cannot reduce O_2 to yield •O_2− (E (O_2/•O_2−) = –0.33 eV)[36], and the holes in the VB of the g-C_3N_4 (+1.57 eV) cannot oxidize H_2O to give •OH (E (•OH/H_2O) = 2.27 eV)[37]. As a result, the holes in the VB of the g-C_3N_4 as the main reactive species can degrade the RhB
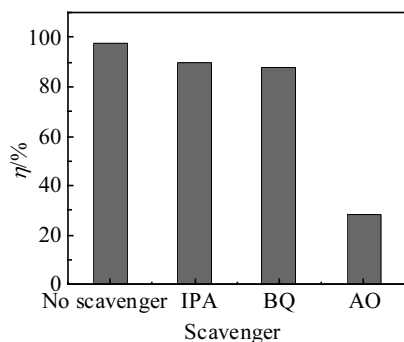
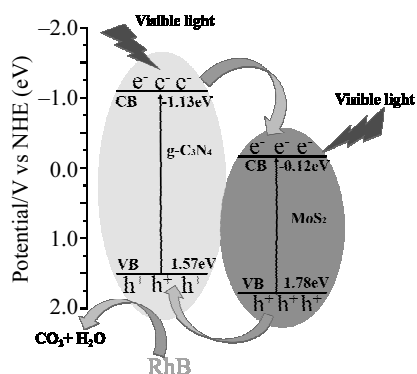Fig.7   Degradation efficiency (η) of RhB in presence of different scavengers under visible light irradiation

Fig.8   Schematic diagram of the photocatalytic degradation and charge transfer mechanism in the MoS_2 nanosheet/g-C_3N_4 heterojunction systems

molecules, which is consistent with the result of adding scavengers. The results are in good agreement with the reported results of Li et al [25].

3   Conclusions

1) The MoS_2 nanosheets/g-C_3N_4 heterojunction can be prepared by a facile ball milling method.

2) The heterojunction shows significantly enhanced photocatalytic performance for the degradation of RhB under visible light irradiation.

3) The enhanced photocatalytic activity is mainly attributed to the efficient separation and transport of photoinduced electron-hole pairs in the heterojunction structure.

References

1   Hoffmann M R, Choi W Y, Bahnemann D W. *Chemical Review* [J], 1995, 95: 69

2   Serpone N, Emeline A V. *Journal of Physical Chemistry Letters* [J], 2012, 3: 673

3   Malato S, Maldonado M I, Fernández-Ibáñez P *et al*. *Materials Science in Semiconductor Processing*[J], 2015, 42(1): 15

4   Li Y S, Tang Z L, Zhang J Y *et al*. *Rare Metal Materials and Engineering*[J], 2015, 44(S1): 361 (in Chinese)

5   Tong H, Zhu Y J, Yang L X *et al*. *Journal of Physical Chemistry C*[J], 2017, 111: 3893

6   Huo F, Wang Y, You C *et al*. *Journal of Materials Science*[J], 2017, 52(10): 5626

7   Meenakshi G, Sivasamy A. *Ecotoxicology and Environmental Safety*[J], 2017, 135: 243

8   Wang X C, Maeda K, Thomas A *et al*. *Nature Materials*[J], 2009, 8: 76

9   Mamba G, Mishra A K. *Applied Catalysis B: Environmental*[J], 2016, 198: 347

10 Yan S C, Li Z S, Zou Z G. *Langmuir*[J], 2009, 25: 10 397

11 Yuan X, Zhou C, Jin Y *et al*. *Journal of Colloid and Interface Science*[J], 2016, 468: 211

12 Jiang D, Chen L, Zhu J *et al*. *Dalton Transactions*[J], 2013, 42: 15 726

13 Fang Z L, Rong H F, Zhou L Y *et al*. *Journal of Materials Science*[J], 2015, 50: 3057

14 Jiang D, Zhu J, Chen M *et al*. *Journal of Colloid and Interface Science*[J], 2014, 417: 115

15 Zhao J, Ji Z, Shen X *et al*. *Ceramics International* [J], 2015, 41: 5600

16 Hu S W, Yang L W, Tian Y *et al*. *Applied Catalysis B: Environmental*[J], 2015, 163: 611

17 Peng W C, Li X Y. *Catalysis Communications*[J], 2014, 49: 63

18 Li Q, Zhang N, Yang Y *et al*. *Langmuir*[J], 2014, 30: 8965

19 Tian Y, Ge L, Wang K *et al*. *Materials Characterization*[J], 2014, 87: 70

20 Zhang W, Xiao X, Li Y *et al*. *Applied Surface Science*[J], 2016, 389: 496

21 Ye L, Wang D, Chen S *et al*. *ACS Applied Materials and Interfaces*[J], 2016, 8: 5280

22 Wang J, Guan Z, Huang J *et al*. *Journal of Materials Chemistry A*[J], 2014, 2: 7960

23 Zhao H, Dong Y, Jiang P *et al*. *Journal of Materials Chemistry A* [J], 2015, 3: 7375

24 Ge L, Han C, Xiao X *et al*. *International Journal of Hydrogen Energy*[J], 2013, 38: 6960

25 Li J, Liu E Z, Ma Y N *et al*. *Applied Surface Science*[J], 2016, 364: 694

26 Lu X, Jin Y, Zhang X *et al*. *Dalton Transactions*[J], 2016, 45: 15 406

27 Hou Y, Wen Z, Cui S *et al*. *Advanced Materials*[J], 2013, 25: 6291

28 Yao Y, Lin Z, Li Z *et al*. *Journal of Materials Chemistry A*[J], 2012, 22: 13 494

29 Shi W, Guo F, Chen J *et al*. *Journal of Alloys and Compounds* [J], 2014, 612: 143

30 Liu W, Wang M, Xu C *et al*. *Journal of Molecular Catalysis A: Chemical*[J], 2013, 368-369: 9

31 Liu L, Qi Y, Yang J *et al*. *Applied Surface Science*[J], 2015, 358: 319

32 Miao H, Zhang G, Hu X *et al*. *Journal of Alloys and Compounds*

[J], 2017, 690: 669

33 Qiu J, Feng Y, Zhang X *et al. RSC Advances*[J], 2017, 7: 10 668

34 Peng W C, Chen Y, Li X Y. *Journal of Hazardous Materials*[J], 2016, 309: 173

35 Jo W K, Lee J Y, Sagaya N C. *Chemical Engineering Journal*[J],

2016, 289: 306

36 Chen X, Tan P, Zhou B *et al. Journal of Alloys and Compounds* [J], 2015, 647: 456

37 Lv H, Ji G, Yang Z *et al. Journal of Colloid and Interface Science*[J], 2015, 450: 381

g-C$_3$N$_4$/MoS$_2$ 纳米片异质复合物的球磨法制备及可见光催化性能

阎　鑫[1]，高　强[1]，惠小艳[1]，闫从祥[1]，艾　涛[1]，王振军[1,2]，孙国栋[1]，苏兴华[1]，赵　鹏[1]

(1. 长安大学，陕西 西安 710064)

(2. 交通铺面材料教育部工程研究中心，陕西 西安 710064)

摘　要：采用球磨法制备 g-C$_3$N$_4$/MoS$_2$ 纳米片异质复合物，运用 X 射线衍射仪、高分辨率透射电镜、紫外可见漫反射光谱和荧光发射光谱对异质复合物的结构和形貌进行了表征。以罗丹明 B 为模拟污染物，在可见光照射下考察了复合物的光催化特性。结果表明：MoS$_2$ 纳米片可进入 g-C$_3$N$_4$ 的层间形成异质复合物。含有 2% MoS$_2$ 纳米片与 g-C$_3$N$_4$ 形成的异质复合物在 120 min 内对罗丹明 B 的降解率为 98%，其降解动力学常数是体相 g-C$_3$N$_4$ 的 4.3 倍。g-C$_3$N$_4$/MoS$_2$ 纳米片异质复合物具有十分优良的光催化特性，其催化活性的提高主要归因于光生电子和空穴的有效分离和传输。根据光捕获实验提出了复合物可能的光催化机理。

关键词：MoS$_2$ 纳米片；石墨相氮化碳；异质复合物；球磨；可见光催化

作者简介：阎　鑫，男，1976 年生，博士，副教授，长安大学材料科学与工程学院，陕西 西安 710064，电话：029-82337340，E-mail: xinyan@chd.edu.cn